Bias-Field Digitized Counterdiabatic Quantum Algorithm for Higher-Order Binary Optimization

Sebastián V. Romero[1,2] Anne-Maria Visuri[1] Alejandro Gomez Cadavid[1,2] Enrique Solano,[1] and Narendra N. Hegade[1,*]

[1]*Kipu Quantum GmbH, Greifswalderstrasse 212, 10405 Berlin, Germany*

[2]*Department of Physical Chemistry, University of the Basque Country UPV/EHU, Apartado 644, 48080 Bilbao, Spain*

(Dated: September 5, 2024)

We present an enhanced bias-field digitized counterdiabatic quantum optimization (BF-DCQO) algorithm to address higher-order unconstrained binary optimization (HUBO) problems. Combinatorial optimization plays a crucial role in many industrial applications, yet classical computing often struggles with complex instances. By encoding these problems as Ising spin glasses and leveraging the advancements in quantum computing technologies, quantum optimization methods emerge as a promising alternative. We apply BF-DCQO with an enhanced bias term to a HUBO problem featuring three-local terms in the Ising spin-glass model. Our protocol is experimentally validated using 156 qubits on an IBM quantum processor with a heavy-hex architecture. In the studied instances, the results outperform standard methods, including the quantum approximate optimization algorithm (QAOA), quantum annealing, simulated annealing, and Tabu search. Furthermore, we perform an MPS simulation and provide numerical evidence of the feasibility of a similar HUBO problem on a 433-qubit Osprey-like quantum processor. Both studied cases, the experiment on 156 qubits and the simulation on 433 qubits, can be considered as the start of the commercial quantum advantage era, Kipu dixit, and even more when extended soon to denser industry-level HUBO problems.

I. INTRODUCTION

Combinatorial optimization problems arise in a multitude of situations in science and industry, from logistics and scheduling to computational chemistry and biology. In combinatorial optimization, the best or near-optimal solution is searched within a finite but large discrete configuration space. Theoretical tools from statistical physics have given insights into these problems, as their connection to disordered systems was identified early on Ref. [1]. These problems generally belong to the NP-hard complexity class, requiring a computation time that grows exponentially with the problem size on classical computers. While complex problem instances test the limits of classical computing, quantum computing has emerged as a suitable counterpart to drive the state-of-the-art in this field. This is brought forward by the rapid development of quantum technologies combined with the natural mapping of combinatorial optimization problems to the widely studied Ising spin glass model, whose ground state encodes the optimal solution [2]. Several methods have been proposed so far, including adiabatic quantum optimization [3] and the QAOA [4], which can be thought as a digitized version of an adiabatic quantum computing procedure [5].

In addition to the capacity of quantum hardware to embed large-scale systems, the potential of quantum computing to surpass classical optimization methods has been demostrated through dedicated quantum algorithms [6–13]. Among these, QAOA has emerged as one of the front-runner candidates for showing quantum speedup in optimization. Recent studies on 8-SAT up to 20 variables [14] show that the time to solution for QAOA outperforms best-known classical methods. Similar evidence of quantum speedup for solving the low autocorrelation binary sequence (LABS) problem has also been found [15–17].

In parallel with quantum algorithms, quantum-inspired algorithms run on classical hardware, especially those based on tensor networks (TNs) [18–22], have evolved rapidly in the recent years. They were developed over the past three decades mostly for the study of condensed-matter physics [21, 23] and have been adopted as efficient simulators of quantum hardware, as classical benchmarks for quantum algorithms, and in hybrid approaches combining TNs and quantum algorithms [24, 25]. The recent kicked-Ising-model experiment of IBM on a 127-qubit device [26–30] and D-Wave's simulation of quantum quench dynamics across a spin-glass phase transition [31, 32] highlighted the interplay of quantum simulations and TNs. For combinatorial optimization, new approaches have combined generative machine learning models with TNs [33–35], and ground-state search methods have been applied to problems with up to quadratic terms on higher-dimensional graphs [36–38].

Compared to quadratic problems, higher-order ones are significantly more difficult to solve. While a number of experiments have recently demonstrated HUBO implementations on quantum hardware [39–41], there are hardware limitations that complicate the effective implementation of these protocols on large- and even intermediate-scale problems. These include short decoherence times, qubit connectivities, and the presence of noise. Several alternative methods, such as counterdiabatic driving (CD) protocols, have been proposed to overcome these issues [42–47]. By suppressing diabatic transitions, CD protocols can find better solutions in different scenarios.

In this work, we exploit the recently developed BF-DCQO formulation [48] to address HUBO problems on both ideal simulators and hardware. Here, we make use of the entire new 156-qubit IBM quantum computer IBM_FEZ [49] and a matrix product state (MPS) simulation of the upcoming IBM Osprey processor with 433 qubits. All results are compared with those obtained through well-established classical optimization methods as well as the D-Wave quantum annealing platform [50], known for solving quadratic unconstrained bi-

* narendrahegade5@gmail.com

nary optimization (QUBO) problems naturally because of its structure. For both methods, extra qubits are needed for mapping HUBO problems into implementable QUBO instances. We furthermore obtain a reference MPS solution using the density matrix renormalization group (DMRG) method for ground-state search [51]. Even though our work addresses problems with up to three-body terms, our main findings can be extended to higher-order optimization problems, including the LABS problem [17], MAX k-SAT [52], factorization [53] and protein folding [54, 55], among others.

II. FORMULATION

A. Digitized counterdiabatic quantum optimization (DCQO)

Adiabatic quantum optimization aims to prepare the ground state of a given problem Hamiltonian. An initial state is evolved within the time window $t \in [0, T]$ under the adiabatic protocol $H_{\rm ad}(\lambda) = (1-\lambda)H_i + \lambda H_f$. Here, $\lambda(t)$ is a time-dependent scheduling function that describes the adiabatic evolution of the system, starting from an initial Hamiltonian H_i, whose corresponding ground state is easy to prepare, towards the problem Hamiltonian H_f. Relying on the adiabatic theorem, this protocol reaches the desired H_f ground state in the adiabatic limit $\dot{\lambda}(t) \to 0$. Following Ref. [48], we extend a disordered Ising Hamiltonian to up to three-body terms:

$$H_f = \sum_i h_i^z \sigma_i^z + \sum_{ij} J_{ij} \sigma_i^z \sigma_j^z + \sum_{ijk} K_{ijk} \sigma_i^z \sigma_j^z \sigma_k^z. \tag{1}$$

The ground state of this Hamiltonian is called a p-spin glass with $p = 3$ [56], and the model is commonly known in quantum optimization as the higher-order Ising chain [39, 40]. In the following, we use $\lambda(t) = \sin^2(\pi \sin^2(\pi t/2T)/2)$ as the scheduling function. We will use as initial Hamiltonian

$$H_i = \sum_j h_j^x \sigma_j^x + \sum_j h_j^b \sigma_j^z \tag{2}$$

with h_j^x (h_j^b) the transverse- (longitudinal bias-) field contributions acting on the jth spin. We set $h_j^x = -1$ and $h_j^b = 0$, so that the N-qubit ground state of H_i is

$$|+\rangle^{\otimes N} = \left(\frac{|0\rangle + |1\rangle}{\sqrt{2}}\right)^{\otimes N}. \tag{3}$$

In order to overcome the intrinsic slow adiabatic evolution, it is possible to introduce an auxiliary counterdiabatic driving contribution which accelerates the original protocol and suppresses diabatic transitions [42, 43]. The transitionless protocol takes the form

$$H_{\rm cd}(\lambda) = H_{\rm ad}(\lambda) + \dot{\lambda} A_\lambda, \tag{4}$$

where A_λ is the adiabatic gauge potential [57]. Nevertheless, its exact implementation is severely impractical due to its many-body structure and the necessity for the knowledge of the full energy spectrum. To overcome these issues, several approximate implementations have been proposed [57–61]. One such proposal is the approximation of the adiabatic gauge potential by a nested-commutator series expansion

$$A_\lambda^{(l} = i \sum_{k=1}^{l} \alpha_k(t) O_{2k-1}(t), \tag{5}$$

where $O_0(t) = \partial_\lambda H_{\rm ad}$ and $O_k(t) = [H_{\rm ad}, O_{k-1}(t)]$. In the limit $l \to \infty$, this expansion converges to the exact gauge potential. The coefficients α_k are obtained by minimizing the action $S_l = \mathrm{tr}[G_l^2]$ with $G_l = \partial_\lambda H_{\rm ad} - i[H_{\rm ad}, A_\lambda^{(l}]$. For simplicity, we consider the first-order ($l = 1$) nested-commutator term (see Appendix A for a step-by-step derivation), which takes the form

$$\begin{aligned} O_1 = -2i\Big[&\sum_i h_i^z \sigma_i^y + \sum_{i<j} J_{ij}(\sigma_i^y \sigma_j^z + \sigma_i^z \sigma_j^y) \\ &+ \sum_{i<j<k} K_{ijk}(\sigma_i^y \sigma_j^z \sigma_k^z + \sigma_i^z \sigma_j^y \sigma_k^z + \sigma_i^z \sigma_j^z \sigma_k^y)\Big]. \end{aligned} \tag{6}$$

Higher-order terms demand significantly more computational resources, and their complexity increases with the system size.

In the fast evolution regime, the adiabatic term $H_{\rm ad}(\lambda)$ in Eq. (4) can be omitted, reducing the number of required quantum gates and thereby decreasing hardware noise, while still maintaining the quality of the solution [48, 55, 62, 63]. This approach is adopted in the present study, where only the CD contribution is considered without compromising performance. The time evolution of such Hamiltonians remains a challenge on current analog quantum platforms, and may even be highly difficult due to the nonstoquasticity [64]. To address this issue, digitized counterdiabatic quantum protocols have been proposed for implementation on digital quantum computers [65]. The resulting time-evolution operator can be decomposed using a first-order Trotter-Suzuki product formula [66] and digitized under a gate-based model approach as follows

$$U(T,0) = \prod_{k=1}^{n_{\rm trot}} \prod_{j=1}^{n_{\rm terms}} \exp\left[-i\gamma_j(k\Delta t)\Delta t H_j\right], \tag{7}$$

where $H_{\rm cd}(t) = \sum_{j=1}^{n_{\rm terms}} \gamma_j(t) H_j$ is encoded in $n_{\rm terms}$ different Pauli operators H_j and $n_{\rm trot}$ are the Trotter steps considered with $\Delta t = T/n_{\rm trot}$. The number of gates required for implementation is reduced by optimally decomposing the desired circuit following Refs. [67, 68]. Furthermore, we set a gate-cutoff threshold $\theta_{\rm cutoff}$ in our experiments, such that any term in absolute value of (7) with an angle magnitude below this threshold is discarded, thus if $|\gamma_j(k\Delta t)\Delta t| \bmod 2\pi < \theta_{\rm cutoff}$ is met. The larger the $\theta_{\rm cutoff}$, the lower is the amount of resources that are required, but the obtained circuit expressivity is also lower. Therefore, it is crucial to select an appropriate value of this parameter to significantly reduce the amount of gates to implement without compromising the quality of the outcomes.

B. Bias-field updating protocol

State initialization is crucial for the performance of quantum optimization routines, where an initial state with a nonzero overlap with the desired final state is advantageous [69, 70]. Several warm-starting techniques have been proposed, where a relaxed version of the problem is solved classically and its solution fed into the quantum algorithm, leveraging the complexity and cost of the quantum routine while ensuring a better performance [71, 72].

In BF-DCQO, the standard DCQO is performed iteratively, where the solution from each iteration serves as the input bias for the next iteration [47, 48, 69]. At each step, the bias field h_i^b for the ith qubit is updated based on the measured longitudinal component of the qubit, $\langle\sigma_i^z\rangle$. This update follows the rule $h_i^b = h_i^b(\langle\sigma_i^z\rangle)$, where the functional form of h_i^b represents the specific bias-field strategy employed. In this work, we explore the following strategies:

- Unsigned antibias(+)/bias(−): $h_i^b = \pm\langle\sigma_i^z\rangle$. This strategy offers bias fields whose strength is exactly the longitudinal component. This is a sensible choice when a qubit is effectively close to an equal superposition, such that there is no clear direction of bias.
- Signed antibias(+)/bias(−): $h_i^b = \pm\,\mathrm{sgn}\,\langle\sigma_i^z\rangle$. This strategy offers bias fields that are equivalent to the effective orientation of the qubit, regardless the magnitude. This is a sensible choice when a qubit has a clear preferred direction of bias.

Once a suitable updating method has been selected, BF-DCQO iteratively measures the final state after time evolution in the computational basis and the longitudinal bias fields h_i^b are updated accordingly. In the following, we set $h_i^b = 0$ for the first bias-field iteration. According to the findings of Ref. [48], modifying the selected updating strategy throughout the entire routine can circumvent local minima and lead to faster convergence. For our results, we use the unsigned bias followed by a final iteration with a weighted signed bias. Specifically, the strength of h_i^b is increased by rescaling $h_i^b \mapsto \text{constant} \times h_i^b$. In our experiments, we rescale by a factor of five to ensure that the magnitude of the bias is significantly larger than the transverse term, restricting the search space near the previous solution. Since the solution provided by DCQO, from the first iteration, samples low-energy states of the spin-glass Hamiltonian [Eq. (1)], the expectation values of local Pauli-z operators can be used as an effective bias in subsequent iterations, facilitating convergence.

The initial Hamiltonian is changed after each bias-field update, so that its ground state also changes and has to be prepared for the circuit execution. The lowest eigenvalue of each $h_i^x\sigma_i^x - h_i^b\sigma_i^z$ term of H_i is given by $\lambda_i^{\min} = -\sqrt{(h_i^b)^2 + (h_i^x)^2}$ with eigenstate $|\tilde{\phi}\rangle_i = [h_i^x, h_i^b + \lambda_i^{\min}]^{\mathrm{T}}$ up to normalization. This product state can be efficiently prepared in a depth-one circuit layer by means of single-qubit y-axis rotations such that

$$|\tilde{\psi}\rangle = \bigotimes_{i=1}^{N} |\tilde{\phi}\rangle_i = \bigotimes_{i=1}^{N} R_y(\theta_i)\,|0\rangle_i \tag{8}$$

with $\theta_i = \tan^{-1}(h_i^x/(h_i^b - \lambda_i^{\min}))$.

Once the circuit has been prepared, all qubits are measured n_{shots} times, returning an N-bitstring $x_0 \ldots x_{N-1}$. Each measurement trivially translates into a sample of H_f due to its construction as a weighted sum of Pauli-z operators. Denoting each of these samples as E_k, the sample mean energy is defined as $E \coloneqq (1/n_{\text{shots}}) \sum_{k=1}^{n_{\text{shots}}} E_k$. It can be used as an estimator of the expectation value of H_f after ground-state preparation.

It has been demonstrated that incorporating Conditional Value-at-Risk (CVaR) techniques on quantum optimization routines [73] can lead to significant improvements. Building upon this knowledge, in this work, we propose a CVaR-inspired method for iteratively updating the bias fields. Accordingly, let α be the ratio between the number of measurements considered and the total number of shots n_{shots}. Rather than taking the entire distribution of samples into account ($\alpha = 1$), we first sort them in terms of energy, thus $E_k \leq E_{k+1}$. Next, the bias is updated using a fraction $0 < \alpha < 1$ of the lowest-energy outcomes taken from

$$E(\alpha) = \frac{1}{\lceil \alpha n_{\text{shots}} \rceil} \sum_{k=1}^{\lceil \alpha n_{\text{shots}} \rceil} E_k, \tag{9}$$

thus taking only a part of the total distribution into account. From the results drawn from both noiseless simulators and hardware, faster convergence to better solutions is expected for values of $\alpha \sim 1\%$.

Apart from seeking a reduction in the resources required and depth of the circuits considered, it is important to quantify the quality of the results obtained by the routines. In order to evaluate the performance of our routines, we use two metrics: the approximation ratio

$$\mathrm{AR} = \frac{E(\alpha = 1)}{E_0}, \tag{10}$$

and the distance to solution

$$\mathrm{DS} = 1 - \frac{\min\{E_k\}_{k=1}^{n_{\text{shots}}}}{E_0}. \tag{11}$$

In all our studies, the reference ground-state energies E_0 are obtained by applying the DMRG algorithm [51] implemented in the ITensor library [74] and sampling over random initial MPSs (see Appendix B).

III. RESULTS

A. HUBO instances considered

In this section, we present the HUBO Hamiltonians that will be employed for testing BF-DCQO. Based on the gate error rates and on the coupling map connectivities of the selected platforms, we work with a nearest-neighbour three-body spin glass. In order to tackle industry-related use cases, we furthermore consider the weighted MAX 3-SAT problem [52]. To the best of our knowledge, this is the first work to

tackle a binary satisfiability problem with the aid of CD protocols. For both cases, the corresponding circuit decomposition is shown in Fig. 5 of Appendix C.

Nearest-neighbour spin glass.—For the first case, the nearest-neighbour (NN) three-body Hamiltonian takes the form of

$$H_f^{\mathrm{NN}} = \sum_i h_i^z \sigma_i^z + \sum_{\langle ij \rangle} J_{ij} \sigma_i^z \sigma_j^z + \sum_{\langle ijk \rangle} K_{ijk} \sigma_i^z \sigma_j^z \sigma_k^z, \tag{12}$$

where $\langle \cdot \rangle$ indicates that the enclosed qubit indices are nearest neighbours (thus $j = i + 1$ and $k = i + 2$). The coupling constants h_i, J_{ij} and K_{ijk} are taken as random Gaussian-distributed numbers with zero mean and unit variance. The first-order nested-commutator expansion for this Hamiltonian is given by Eq. (6) but it only contains the nearest-neighbour qubit indices as in Eq. (12). Due to its linearity, it perfectly sticks to the heavy-hex IBM qubit coupling maps. Furthermore, the ease with which this and related models can be simulated using tensor networks makes their simulation an ideal benchmark for evaluating the performance of quantum platforms. Additionally, we conduct a similar test considering a 433-qubit NN HUBO instance, with the objective of simulating ideally (without noise) the expected performance of the upcoming IBM Osprey quantum platform via MPS. For this case, the values $n_{\mathrm{shots}} = 10000$, $\alpha = 0.01$, $\theta_{\mathrm{cutoff}} = 0.06$ are set. The results can be seen in Fig. 1, with the amount of resources needed per iteration shown in Table I.

Weighted MAX 3-SAT problem.—The maximum k-satisfiability (MAX k-SAT) problem belongs to the NP-complete complexity class [75] and its weighted variant is defined as follows: given a Boolean formula in conjunctive normal form (thus conjunction of disjuncted clauses), the weighted maximum k-satisfiability problem (MAX W-k-SAT) aims to find an assignment of truth-valued variables that maximizes the sum of weights of all the k-variable clauses met [52]. The MAX k-SAT problem can be recovered simply by setting the weights be equal to one. If we let $k = 3$, this problem can be written as

$$C^{\mathrm{MW3S}}(l) = \bigwedge_{ijk} \omega_{ijk} l_i \vee l_j \vee l_k, \tag{13}$$

with l_i a literal representing a propositional variable, either u_i or its negation $\bar{u}_i$, and ω_{ijk} are the weights. The problem can be mapped into binary variables by performing the substitution $u_i \mapsto 1 - x_i$ and $\bar{u}_i \mapsto x_i$ with $x_i \in \{0, 1\}$. For each clause, the OR product of literals can be expanded into products of binary variables, e.g.

$$u_i \vee \bar{u}_j \vee u_k \mapsto (1 - x_i) x_j (1 - x_k). \tag{14}$$

In order to address this problem with the aid of quantum computers, we perform an additional map turning the binary variables into Ising variables using the transformation $x_i \mapsto (I - \sigma_i^z)/2$.

Setting $c_i = 1$ if l_i is negated and $c_i = 0$ otherwise, we finally define the problem Hamiltonian as

$$H_f^{\mathrm{MW3S}} = \sum_{ijk} \frac{\omega_{ijk}}{8} [I + (-1)^{c_i} \sigma_i^z][I + (-1)^{c_j} \sigma_j^z][I + (-1)^{c_k} \sigma_k^z]. \tag{15}$$

Here, ω_{ijk} is chosen as a random uniformly distributed variable between zero and one. As it is a maximization problem, it can be transformed into a minimization one by performing the map $H_f^{\mathrm{MW3S}} \mapsto -H_f^{\mathrm{MW3S}}$. The first-order nested-commutator of Eq. (15) yields

$$\begin{aligned} O_1^{\mathrm{MW3S}} = -i \sum_{ijk} \frac{\omega_{ijk}}{4} \Big[& (-1)^{c_i} \sigma_i^y [I + (-1)^{c_j} \sigma_j^z][I + (-1)^{c_k} \sigma_k^z] \\ & + (-1)^{c_j} [I + (-1)^{c_i} \sigma_i^z] \sigma_j^y [I + (-1)^{c_k} \sigma_k^z] \\ & + (-1)^{c_k} [I + (-1)^{c_i} \sigma_i^z][I + (-1)^{c_j} \sigma_j^z] \sigma_k^y \Big]. \end{aligned} \tag{16}$$

It can be seen that MAX W-3-SAT is in general a highly nonlocal Hamiltonian and thus is challenging to implement. We consider here the NN version of the MAX W-3-SAT Hamiltonian of Eq. (15), where consecutive indices are summed over as in Eq. (12). This model is similar to the nearest-neighbour spin-glass Hamiltonian H_f^{NN} but with additional next-to-nearest neighbour terms, namely $\sigma_i^z \sigma_{i+2}^z$, which makes it more complex to implement. In essence, this is due to the fact that such terms are seen as three-body interactions for a heavy-hex lattice, where an additional number of entangling gates are needed to couple distant qubits.

In contrast to physical phase transitions where variations of the system parameters lead to qualitative changes in its properties, in computer science, computational phase transitions occur at critical points where algorithms require an increasing amount of computational resources, becoming less and less tractable [76]. The computational phase transitions of k-SAT have been the subject of several works [76–78]. They depend critically on the density of the problem, i.e., the ratio between its clauses and variables.

B. Comparison of methods

In the following lines, we perform a comparison of both the original BF-DCQO approach [48] and our novel proposed variant, conducting a 433-qubit study using a NN HUBO instance [Eq. (12)] via MPS with which to simulate the expected performance of the upcoming IBM Osprey quantum platform without noise. For this case, the values $n_{\mathrm{shots}} = 10000$ and $\theta_{\mathrm{cutoff}} = 0.06$ are set for both approaches and $\alpha = 0.01$ for our variant. The results can be seen in Fig. 1 with the amount of resources needed per iteration in Table I.

Figure 1 shows that before applying the signed bias, we obtain a 10.6% enhancement of the AR and 60.8% for the DS, demonstrating that our novel CVaR-based approach for updating the bias fields provides a better performance than standard BF-DCQO. After the signed bias method is applied for the last iteration, these values increases to 34.4% and 87.3%, respectively, showing that this additional feature also remarkably contributes to improving the results obtained from standard BF-DCQO.

In addition, we find as an intrinsic signature of our BF-DCQO variant that the circuits implemented for each iteration require less and less resources even though the outcomes

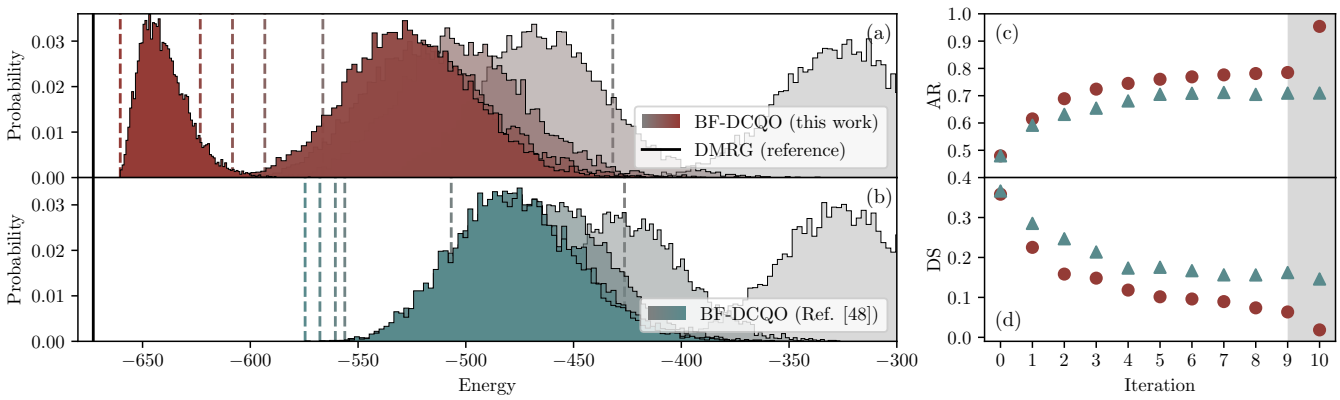

FIG. 1. 433-qubit NN HUBO results on IBM Osprey simulated via MPS. (a) Energy distributions for iterations 0, 2, 4, 6, 8 and 10; from grey to maroon using our novel BF-DCQO variant. The continuous line corresponds to the reference ground-state energy E_0 given by DMRG, and the dashed lines correspond to the minima obtained from the distributions. (b) Same plot as (a), going from grey to teal, but considering the original BF-DCQO approach [48]. (c)-(d) Approximation ratios and distances to solution obtained for each iteration for both approaches. For both panels and only for our variant (maroon markers), the shaded area indicates that the bias update is changed from unsigned to signed bias in the last iteration. See Table I.

TABLE I. Resources needed and results obtained per BF-DCQO iteration to optimize via MPS a 433-qubit NN HUBO with $n_{\text{shots}} = 10000$ and $\theta_{\text{cutoff}} = 0.06$ for both our BF-DCQO variant (left columns) and the original approach (right columns). For our variant, we used $\alpha = 0.01$ and we perform a signed bias in the last iteration.

Iteration	X		$\sqrt{X}$		RZ(θ)		CZ		Depth		AR		DS	
0	497	497	5910	5910	5934	5934	2275	2275	99	99	0.480	0.480	0.358	0.366
1	470	453	5563	5421	5525	5379	2156	2108	98	98	0.615	0.592	0.225	0.285
2	466	446	5412	5310	5365	5247	2106	2066	98	98	0.689	0.632	0.158	0.247
3	436	427	5314	5314	5254	5261	2063	2065	98	98	0.724	0.654	0.148	0.214
4	455	441	5283	5310	5240	5242	2052	2063	98	98	0.745	0.681	0.118	0.173
5	479	450	5287	5310	5238	5251	2052	2063	98	98	0.760	0.705	0.102	0.175
6	474	448	5287	5301	5247	5207	2052	2061	99	98	0.769	0.709	0.096	0.167
7	455	435	5283	5301	5198	5226	2052	2061	98	99	0.776	0.712	0.089	0.156
8	464	456	5283	5310	5210	5251	2052	2063	98	98	0.781	0.705	0.074	0.156
9	447	447	5284	5277	5210	5214	2052	2052	99	98	0.785	0.709	0.064	0.162
10	100	456	1879	5283	1653	5225	496	2052	80	97	0.954	0.710	0.019	0.146

are more optimal. Conceptually, the goal of BF-DCQO is to encode the ground state of H_f, which is a product state in the computational basis. As this is a separable state with no entanglement, BF-DCQO pushes the energy distribution towards the preparation of this state, thereby reducing the amount of entanglement required per iteration.

In order to assess the potential of our proposed BF-DCQO variant, we conduct a comprehensive benchmark study comparing it against several well-established classical optimization techniques as well as the D-Wave platform. In particular, we optimize the nearest-neighbour three-body spin glass of Eq. (12) using a 156-qubit instance.

The results are presented in Fig. 2, where the methods and parameters are given by:

- Simulated annealing (SA) and Tabu search (TS) both with $n_{\text{shots}} = 100000$.
- D-Wave quantum annealers (DW) using Advantage_system4.1 [50] with an annealing time of 2000 µs and $n_{\text{shots}} = 100000$. Based on Ref. [40], we set a coupling strength that is two times the largest coupling of Eq. (1) in absolute value. We thereby introduce a penalty term after the HUBO-into-QUBO mapping when a product constraint is not met in the corresponding reduced spin glass model.
- Tenth iteration of BF-DCQO [48], with $\alpha = 0.02$ run on ibm_fez using $\theta_{\text{cutoff}} = 0.06$, $n_{\text{trot}} = 3$ and $n_{\text{shots}} = 10000$. Previously, the ten BF-DCQO iterations were simulated using MPS without noise.
- CVaR-QAOA [4, 73] with $p = 3$ layers, $n_{\text{shots}} = 10000$ and $\alpha = 0.1$ via MPS using the SPSA optimizer.
- The DMRG implementation of the ITensor library [74] setting 5 sweeps, maximum bond dimensions of $[5, 10, 10, 10, 20]$ and a truncation error cutoff of 10^{-5} (see Appendix B). We sample over 100 random MPS initial states with bond dimension $\chi = 5$ and select the best outcome.

Figure 2 illustrates that BF-DCQO is capable of outperforming other established methods on current noisy quantum platforms, returning an energy distribution whose minimum

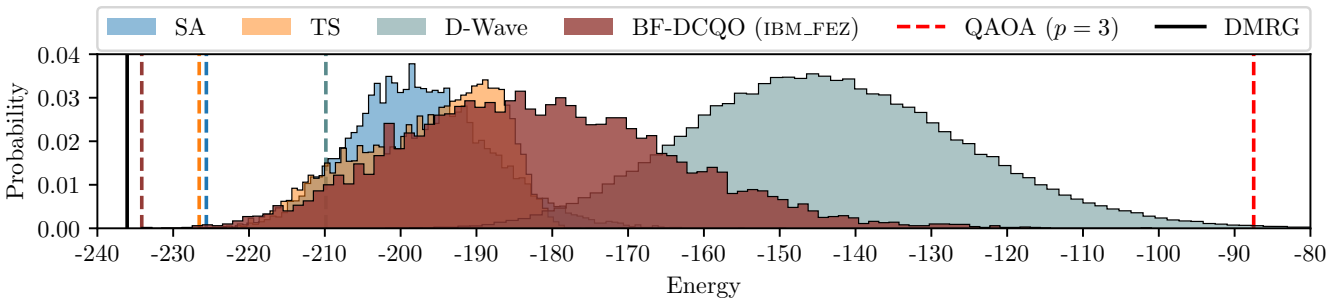

FIG. 2. 156-qubit NN HUBO instance described by Eq. (12) under different approaches: simulated annealing (SA, blue), Tabu search (TS, orange), D-Wave (green), BF-DCQO om IBM_FEZ (purple), and the best outcome of QAOA up to $p = 3$ layers (dashed red). The DMRG optimal solution is used as a ground state reference (black line). The dashed vertical lines indicate the minimum energy values obtained for each approach. The D-Wave and BF-DCQO distributions correspond to experiments run on quantum hardware.

outcome is very close to the ground state reference provided by DMRG. In particular, we have obtained a 26.7% enhancement of the AR and 92.7% of the DS metrics with respect to D-Wave and a 72.8% enhancement of DS for SA approach but a small −8.0% lowering for the AR metric. Despite the fact that three layers were chosen for CVaR-QAOA to recover the expected behaviour of BF-DCQO with $n_{\text{trot}} = 3$, the obtained results show the worst performance, even in comparison with D-Wave. This finding is in accordance with the results presented in Ref. [40]. Furthermore, it should be noted that BF-DCQO and QAOA are the only approaches that do not suffer from the inherent qubit overhead required by the rest of the methods considered for mapping HUBO into QUBO problems. In addition, as the order of many-body terms in the problem Hamiltonian H_f increases, the qubit overhead increases and more resources are required. In particular, regular quadratization methods require a number of ancillary qubits proportional to $n_{k\text{-body}}(k-2)$, with $n_{k\text{-body}}$ the number of k-body terms of H_f [79–81]. Therefore, a worse performance is expected. Other known methods such as Gurobi [82] and CPLEX [83] also suffer from this drawback. For the results presented in Fig. 2, 334 variables were needed for SA, TS and D-Wave. This feature is absent in BF-DCQO, making it a suitable technique for working with large-scale optimization problems with minimal resource requirements.

Up to this point, we have compared the performance of BF-DCQO on quantum hardware using only the last iteration of the entire routine simulated via MPS. In the following section, the impact of running the entire routine under noisy environments is examined. To this end, larger values of θ_{cutoff} will be set in order to guarantee implementability. We note that considering a larger number of measurements might allow us to partially recover the lost expressivity due to the increase of θ_{cutoff}.

C. Hardware implementation on IBM

We first make use of the 156-qubit superconducting quantum platform IBM_FEZ with the native gate set $\{X, \sqrt{X}, \text{RZ}(\theta), \text{CZ}\}$ (see Appendix C). The linearity of its heavy-hex qubit coupling map encourages us to work with Hamiltonians whose many-body terms are nearest neighbours, thereby avoiding an overhead of entangling gates for coupling distant qubits. With this in mind, we solve the same 156-qubit NN HUBO instance that was previously tested in Fig. 2, but we now run the entire routine on IBM_FEZ. The computation is thus conducted in a purely quantum manner. We use $n_{\text{shots}} = 10000$, $\alpha = 0.01$, $\theta_{\text{cutoff}} = 0.13$ and a total of eleven iterations, considering an unsigned-bias update for the first ten and a signed bias for the last one. The results are presented in Fig. 3, which depicts the iterative procedure of BF-DCQO and how the obtained outcomes move towards the desired solution. The amount of resources needed per iteration is given in Table II. As a final remark, the final iteration of the purely quantum BF-DCQO routine exhibits a slightly worse performance when compared to the results of Fig. 2, which employed a noiseless simulation with a considerably lower gate threshold. The purely quantum BF-DCQO still outperforms the optimal solution obtained on the D-Wave platform, where we obtained 34.1% of AR enhancement and 66.4% of DS enhancement with respect the experiment run on D-Wave in Fig. 2.

With the aim of solving more industrially relevant and denser large-scale problems, we also solve a 156-qubit NN MAX W-3-SAT instance on IBM_FEZ, described by Eq. (15)

TABLE II. Resources needed and results obtained per BF-DCQO iteration on IBM_FEZ to optimize a 156-qubit HUBO with $n_{\text{shots}} = 10000$, $\alpha = 0.01$ and $\theta_{\text{cutoff}} = 0.13$. At the last iteration, we performed signed bias.

Iteration	X	$\sqrt{X}$	RZ(θ)	CZ	Depth	AR	DS
0	115	1020	1030	477	129	0.274	0.397
1	86	969	916	430	126	0.373	0.344
2	92	958	869	424	129	0.415	0.261
3	85	937	861	410	124	0.470	0.224
4	93	938	862	410	127	0.495	0.176
5	83	941	878	410	124	0.458	0.226
6	85	940	878	410	125	0.499	0.187
7	79	899	834	386	90	0.514	0.203
8	79	903	835	386	93	0.484	0.245
9	79	941	859	410	130	0.494	0.218
10	3	330	180	13	39	0.815	0.037

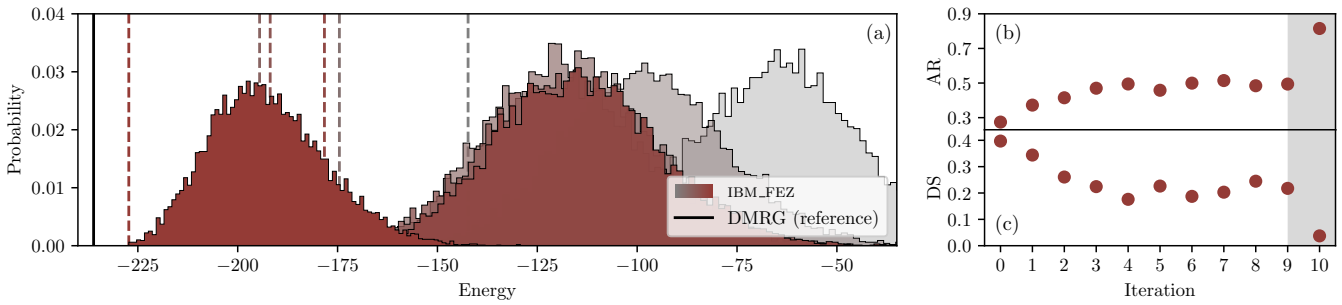

FIG. 3. 156-qubit NN HUBO results on IBM_FEZ. (a) Energy distributions for iterations 0, 2, 4, 6, 8 and 10; from grey to maroon respectively. The continuous line corresponds to the reference ground state E_0 given by DMRG. The dashed lines correspond to the minima obtained from the distributions. (b)-(c) Approximation ratios and distances to solution for each iteration. For both panels, the shaded area indicates that the bias update is changed from unsigned to signed bias in the last iteration. See Table II.

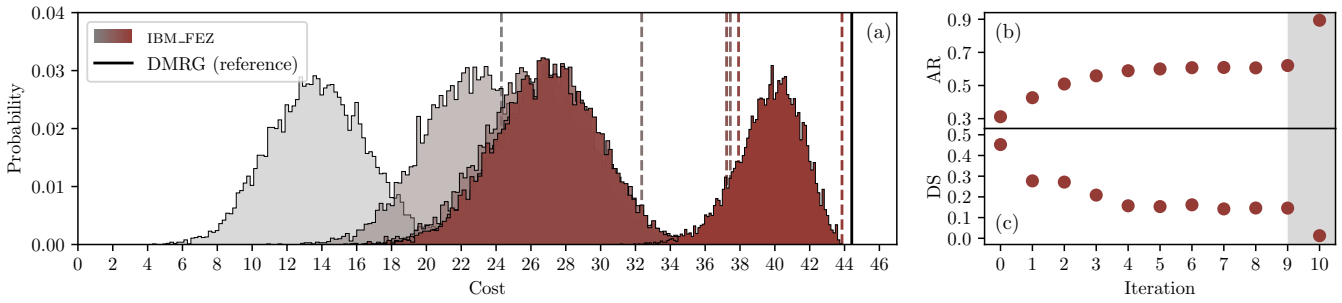

FIG. 4. 156-qubit MAX W-3-SAT HUBO results on IBM_FEZ. (a) Energy distributions for iterations 0, 2, 4, 6, 8 and 10; from grey to maroon respectively. The continuous line corresponds to the reference ground-state energy E_0 given by DMRG. The dashed lines correspond to the maxima of the distributions. (b)-(c) Approximation ratios and distances to solution obtained for each iteration. The shaded area indicates that the bias update is changed from unsigned to signed in the last iteration. See Table III.

TABLE III. Resources needed and results obtained per BF-DCQO iteration on IBM_FEZ to optimize a 156-qubit NN MAX W-3-SAT HUBO problem with $n_{\text{shots}} = 10000$, $\alpha = 0.01$, and $\theta_{\text{cutoff}} = 0.06$. In the last iteration, we apply a signed bias, where no entangling gates are used.

Iteration	X	$\sqrt{X}$	RZ(θ)	CZ	Depth	AR	DS
0	88	1359	1309	495	189	0.311	0.453
1	39	949	808	285	103	0.426	0.277
2	2	450	296	64	23	0.509	0.271
3	3	427	271	56	23	0.559	0.209
4	0	421	267	50	23	0.589	0.157
5	2	411	265	50	19	0.600	0.153
6	2	416	267	50	23	0.608	0.162
7	2	417	263	50	23	0.609	0.142
8	2	412	252	50	18	0.606	0.146
9	2	417	261	50	22	0.621	0.146
10	-	311	156	-	4	0.894	0.013

with only nearest-neighbour terms. We use the same parameters as for the previous instance but change $\theta_{\text{cutoff}} = 0.06$ for convenience. The results are shown in Fig. 4, and the amount of resources needed per iteration is listed in Table III. For this particular problem, the best outcome obtained is remarkably close to the optimal solution despite a purely quantum routine, which highlights the efficacy of BF-DCQO under noisy environments. Additionally, we solved the same HUBO instance on D-Wave using $n_{\text{shots}} = 100000$, where again the purely quantum BF-DCQO outperforms their results, where we obtained 43.0% of AR enhancement and 88.5% of DS enhancement with respect the experiment run on the D-Wave platform.

IV. CONCLUSION

In this study, we investigate and evaluate the performance of novel variants of the recently proposed BF-DCQO algorithm [48] by solving large-scale HUBO instances on IBM quantum processors. The superiority of our BF-DCQO variant over well-established classical techniques and optimization on D-Wave is verified through computing the approximation ratio and the distance to solution in an iterative process. We obtain better optimal solutions while the circuits after each iteration demand less resources. Furthermore, in order to address not only the current but also the near-term hardware, we examine the expected performance of BF-DCQO on the upcoming IBM Osprey platform with 433 qubits. Simulating 433-qubit HUBO instances without noise yields promising results. The BF-DCQO algorithm does not require any classical optimization subroutines, thus avoiding potential trainability drawbacks, nor does it require extra qubits for mapping the initial HUBO into a QUBO problem. It thus emerges as a suitable algorithm for solving higher-order binary optimiza-

tion problems on both current and near-term quantum platforms. We believe that with these results it is fair to claim that the commercial quantum advantage era has started.

ACKNOWLEDGMENTS

We thank Anton Simen Albino, Gaurav Dev and Balaganchi A. Bhargava for fruitful discussions. We acknowledge the use of IBM Quantum services for this work. The views expressed are those of the authors and do not reflect the official policy or position of IBM or the IBM Quantum team.

Appendix A: First-order nested commutator calculation

In order to include the counterdiabatic driving contribution into our protocol, we have to perform the map $H_{\rm ad}(\lambda) \mapsto H_{\rm ad}(\lambda) + \dot{\lambda}\alpha_1(\lambda)O_1(\lambda)$ with $O_k = [H_{\rm ad}(\lambda), O_{k-1}(\lambda)]$ starting from $O_1(\lambda) = [H_{\rm ad}(\lambda), \partial_\lambda H_{\rm ad}(\lambda)] = [H_i, H_f]$ and $\alpha_1(\lambda) = -\Gamma_1(\lambda)/\Gamma_2(\lambda)$ with $\Gamma_k(\lambda) = \mathrm{tr}[O_k^\dagger(\lambda)O_k(\lambda)]$. We start by computing

$$O_1(\lambda) = -2i\sum_i h_i^x h_i^z \sigma_i^y - 2i\sum_{i<j} J_{ij}(h_i^x \sigma_i^y \sigma_j^z + h_j^x \sigma_i^z \sigma_j^y) - 2i\sum_{i<j<k} K_{ijk}(h_i^x \sigma_i^y \sigma_j^z \sigma_k^z + h_j^x \sigma_i^z \sigma_j^y \sigma_k^z + h_k^x \sigma_i^z \sigma_j^z \sigma_k^y). \tag{A1}$$

Next, we compute $\Gamma_1(\lambda)$ as

$$\Gamma_1(\lambda) = \mathrm{tr}[O_1^\dagger(\lambda)O_1(\lambda)] = 4\Big[\sum_i (h_i^x h_i^z)^2 + \sum_{i\neq j}(h_i^x)^2 J_{ij}^2 + \sum_{i<j<k} K_{ijk}^2[(h_i^x)^2 + (h_j^x)^2 + (h_k^x)^2]\Big] \tag{A2}$$

Following the same procedure for computing $\Gamma_2(\lambda)$ and finally taking the squared norm of each separated Pauli string, we obtain

$$\begin{aligned}
\Gamma_2(\lambda) = {} & 16\sum_i (h_i^x)^2\Big[(1-\lambda)h_i^b h_i^z + \lambda\Big((h_i^z)^2 + \sum_{j\neq i} J_{ij}^2 + \sum_{j,k\neq i} K_{ijk}^2\Big)\Big]^2 \\
& + 16\sum_{i<j}(h_i^x)^2\Big[(1-\lambda)J_{ij}h_i^b + 2\lambda\Big(J_{ij}h_i^z + \sum_{i<k<j} K_{ikj}J_{ik} + \sum_{k>j} K_{ijk}J_{ik} + \sum_{k<i} K_{kij}J_{ki}\Big)\Big]^2 \\
& + 16\sum_{i<j}(h_j^x)^2\Big[(1-\lambda)J_{ij}h_j^b + 2\lambda\Big(J_{ij}h_j^z + \sum_{i<k<j} K_{ikj}J_{kj} + \sum_{k>j} K_{ijk}J_{jk} + \sum_{k<i} K_{kij}J_{kj}\Big)\Big]^2 \\
& + 16(1-\lambda)^2\Big[\sum_i (h_i^x)^4 (h_i^z)^2 + \sum_{i<j}[(h_i^x)^2 + (h_j^x)^2]^2 J_{ij}^2 + \sum_{i<j<k} K_{ijk}^2[(h_i^x)^2 + (h_j^x)^2 + (h_k^x)^2]^2\Big] \\
& + 64(1-\lambda)^2\Big[\sum_{i<j}(h_i^x)^2(h_j^x)^2 J_{ij}^2 + \sum_{i<j<k} K_{ijk}^2[(h_i^x)^2(h_j^x)^2 + (h_i^x)^2(h_k^x)^2 + (h_j^x)^2(h_k^x)^2]\Big] \\
& + 16\sum_{i<j<k}(h_i^x)^2\Big[(1-\lambda)K_{ijk}h_i^b + 2\lambda\Big(J_{ij}J_{ik} + K_{ijk}h_i^z + \sum_{j<p<k} K_{ijp}K_{ipk} + \sum_{i<p<j} K_{ipj}K_{ipk} \\
& \qquad + \sum_{p<i} K_{pij}K_{pjk} + \sum_{p>k} K_{ijp}K_{ikp}\Big)\Big]^2 \\
& + 16\sum_{i<j<k}(h_j^x)^2\Big[(1-\lambda)K_{ijk}h_j^b + 2\lambda\Big(J_{jk}J_{ij} + K_{ijk}h_j^z + \sum_{j<p<k} K_{ijp}K_{jpk} + \sum_{i<p<j} K_{ipj}K_{pjk} \\
& \qquad + \sum_{p<i} K_{pij}K_{pjk} + \sum_{p>k} K_{ijp}K_{jkp}\Big)\Big]^2 \\
& + 16\sum_{i<j<k}(h_k^x)^2\Big[(1-\lambda)K_{ijk}h_k^b + 2\lambda\Big(J_{ik}J_{jk} + K_{ijk}h_k^z + \sum_{j<p<k} K_{ipk}K_{jpk} + \sum_{i<p<j} K_{ipk}K_{pjk} \\
& \qquad + \sum_{p<i} K_{pik}K_{pjk} + \sum_{p>k} K_{ikp}K_{jkp}\Big)\Big]^2 \\
& + 64\lambda^2\sum_{i<j<k<p}[(h_i^x)^2(K_{ikp}J_{ij} + K_{ijp}J_{ik} + K_{ijk}J_{ip})^2 + (h_j^x)^2(K_{jkp}J_{ij} + K_{ijp}J_{jk} + K_{ijk}J_{jp})^2 \\
& \qquad + (h_k^x)^2(K_{jkp}J_{ik} + K_{ikp}J_{jk} + K_{ijk}J_{kp})^2 + (h_p^x)^2(K_{jkp}J_{ip} + K_{ikp}J_{jp} + K_{ijp}J_{kp})^2] \\
& + 64\lambda^2\sum_{i<j<k<p<q}[(h_i^x)^2(K_{ijk}K_{ipq} + K_{ikq}K_{ijp} + K_{ikp}K_{ijq})^2 + (h_j^x)^2(K_{ijk}K_{jpq} + K_{ijp}K_{jkq} + K_{ijq}K_{jkp})^2 \\
& \qquad + (h_k^x)^2(K_{ijk}K_{kpq} + K_{ikp}K_{jkq} + K_{ikq}K_{jkp})^2 + (h_p^x)^2(K_{ijp}K_{kpq} + K_{ikp}K_{jpq} + K_{ipq}K_{jkp})^2 \\
& \qquad + (h_q^x)^2(K_{ijq}K_{kpq} + K_{ikq}K_{jpq} + K_{ipq}K_{jkq})^2].
\end{aligned} \tag{A3}$$

Appendix B: DMRG-based estimation of ground state energies

To obtain the reference ground state energy of the nearest-neighbour Hamiltonian of Eq. (12), we employ the DMRG algorithm [51], which is an optimization method using a matrix product state (MPS) as a variational ansatz. Due to entanglement area laws [84], DMRG works particularly well for one-dimensional systems described by MPSs and for local Hamiltonians. We use the implementation in the ITensor Julia library [74]. As initial states, use random MPSs with bond dimension $\chi > 1$ since setting the initial bond dimension to 1 results in higher ground state energies. Even though the exact ground state is a product state (bitstring in the computational basis), we find that the algorithm converges to an entangled state with bond dimension larger than 1. This is indicated by non-integer values of the occupation probabilities $\langle n_i \rangle$. To obtain an estimate for the ground state energy, we adopt the following procedure:

1. Obtain the ground state $|\psi_{\mathrm{DMRG}}\rangle$ via DMRG.
2. For all qubits, measure the occupation probability
$$\langle n_i \rangle = \langle \psi_{\mathrm{DMRG}} | n_i | \psi_{\mathrm{DMRG}} \rangle = \frac{1 - \langle \sigma_i^z \rangle}{2}, \tag{B1}$$
where $0 \leq \langle n_i \rangle \leq 1$.
3. Construct an estimate of the ground-state bit string $|\psi_{\mathrm{GS}}\rangle$ by rounding $\langle n_i \rangle$ to the nearest integer.
4. Compute an estimate of the ground-state energy ϵ_{min} by applying $H_f |\psi_{\mathrm{GS}}\rangle = \epsilon_{\mathrm{min}} |\psi_{\mathrm{GS}}\rangle$.
5. Choose the smallest ϵ_{min} out of the values found for 100 random initial states with bond dimension $\chi = 5$.

Note that the random coupling constants are fixed, i.e. there is no averaging over disorder configurations. Therefore, we select the minimum energy obtained by sampling over 100 randomly generated initial MPSs. The ground-state-energy estimate computed in this way is lower than the energy of each $|\psi_{\mathrm{DMRG}}\rangle$.

The DMRG algorithm is known to be particularly efficient when the Hamiltonian has an exact MPO representation with a small bond dimension [51]. This occurs for Hamiltonians with short-range coupling terms such as considered here, or exponentially decaying ones. The convergence of DMRG, as a variational method, may however be prevented by the algorithm getting stuck in local minima. We observe this here as the state that DMRG converges to is slightly entangled rather than the product state describing a classical spin glass. For small system sizes up to 28 qubits, the DMRG result agrees with the exact one $|\psi_{\mathrm{exact}}\rangle$ with a maximum error $1 - |\langle \psi_{\mathrm{exact}} | \psi_{\mathrm{DMRG}} \rangle|^2 \lesssim 10^{-5}$. We also verify that the product state obtained by rounding $\langle n_i \rangle$ to the nearest integer matches $|\psi_{\mathrm{exact}}\rangle$ in this case.

In previous DMRG studies of classical spin glasses, a quantum wavefunction annealing method was found to improve convergence [85, 86]. As an alternative to DMRG, the ground state search can be performed by imaginary time evolution. This approach was recently used for solving QUBO problems via projected entangled pair states with flexible geometry [38].

Appendix C: Circuit decomposition

An important aspect of preparing and running quantum circuits on hardware is to transpile the required quantum operations according to the corresponding native gate sets provided by the platform. These typically consist of an universal gate set containing several one-qubit gates and a single two-qubit entangling gate. For IBM_FEZ, its native gate set is composed by
$$X = \begin{bmatrix} 0 & 1 \\ 1 & 0 \end{bmatrix}, \quad \sqrt{X} = \frac{1}{2} \begin{bmatrix} 1+i & 1-i \\ 1-i & 1+i \end{bmatrix}, \quad \mathrm{RZ}(\theta) = e^{-i\frac{\theta}{2}\sigma^z}, \tag{C1}$$
with the entangling gate $\mathrm{CZ} = \mathrm{diag}(1, 1, 1, -1)$.

The constrained connectivity among qubits of IBM_FEZ, and quantum platforms with heavy-hex coupling maps in general, suggests to work with highly sparse problems. The linearity of the Hamiltonians considered naturally fits into the heavy-hex IBM qubit coupling maps, whose corresponding circuit decomposition can be seen in Fig. 5.

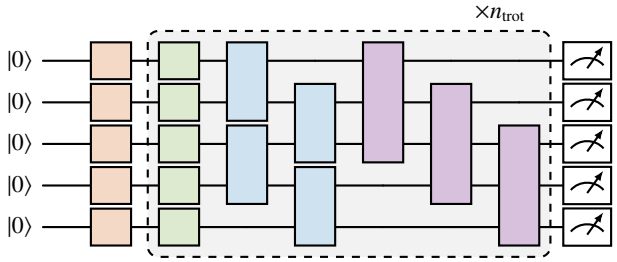

FIG. 5. Circuit decomposition of a five-qubit NN HUBO instance [Eq. (1)]. The first one-qubit operator layer prepares the initial ground state $|\tilde{\psi}\rangle = \bigotimes_{i=1}^{N} R_y(\theta_i) |0\rangle_i$. Afterwards, n_{trot} Trotter steps are applied to implement the digitized time-evolution operator of Eq. (7). Finally, all qubits are measured, and their energy distribution is used for updating the bias field of the subsequent iteration.

[1] Y. Fu and P. W. Anderson, Application of statistical mechanics to NP-complete problems in combinatorial optimisation, Journal of Physics A: Mathematical and General **19**, 1605 (1986).

[2] A. Lucas, Ising formulations of many NP problems, Frontiers in Physics **2**, 10.3389/fphy.2014.00005 (2014).

[3] T. Albash and D. A. Lidar, Adiabatic quantum computation, Rev. Mod. Phys. **90**, 015002 (2018).

[4] E. Farhi, J. Goldstone, and S. Gutmann, A Quantum Approximate Optimization Algorithm (2014), arXiv:1411.4028 [quant-ph].

[5] R. Barends, A. Shabani, L. Lamata, J. Kelly, A. Mezzacapo, U. L. Heras, R. Babbush, A. G. Fowler, B. Campbell, Y. Chen, Z. Chen, B. Chiaro, A. Dunsworth, E. Jeffrey, E. Lucero, A. Megrant, J. Y. Mutus, M. Neeley, C. Neill, P. J. J. O'Malley, C. Quintana, P. Roushan, D. Sank, A. Vainsencher, J. Wenner, T. C. White, E. Solano, H. Neven, and J. M. Martinis, Digitized adiabatic quantum computing with a superconducting circuit, Nature **534**, 222–226 (2016).

[6] C. Durr and P. Hoyer, A Quantum Algorithm for Finding the Minimum (1999), arXiv:quant-ph/9607014 [quant-ph].

[7] A. Montanaro, Quantum-Walk Speedup of Backtracking Algorithms, Theory of Computing **14**, 1 (2018).

[8] A. Montanaro, Quantum speedup of branch-and-bound algorithms, Phys. Rev. Res. **2**, 013056 (2020).

[9] S. Chakrabarti, P. Minssen, R. Yalovetzky, and M. Pistoia, Universal Quantum Speedup for Branch-and-Bound, Branch-and-Cut, and Tree-Search Algorithms (2022), arXiv:2210.03210 [quant-ph].

[10] R. D. Somma, S. Boixo, H. Barnum, and E. Knill, Quantum Simulations of Classical Annealing Processes, Phys. Rev. Lett. **101**, 130504 (2008).

[11] P. Wocjan and A. Abeyesinghe, Speedup via quantum sampling, Phys. Rev. A **78**, 042336 (2008).

[12] M. B. Hastings, A Short Path Quantum Algorithm for Exact Optimization, Quantum **2**, 78 (2018).

[13] A. M. Dalzell, N. Pancotti, E. T. Campbell, and F. G. Brandão, Mind the Gap: Achieving a Super-Grover Quantum Speedup by Jumping to the End, in *Proceedings of the 55th Annual ACM Symposium on Theory of Computing*, STOC 2023 (Association for Computing Machinery, New York, NY, USA, 2023) p. 1131–1144.

[14] S. Boulebnane and A. Montanaro, Solving boolean satisfiability problems with the quantum approximate optimization algorithm (2022), arXiv:2208.06909 [quant-ph].

[15] A. Boehmer, Binary pulse compression codes, IEEE Transactions on Information Theory **13**, 156 (1967).

[16] M. Schroeder, Synthesis of low-peak-factor signals and binary sequences with low autocorrelation (Corresp.), IEEE Transactions on Information Theory **16**, 85 (1970).

[17] R. Shaydulin, C. Li, S. Chakrabarti, M. DeCross, D. Herman, N. Kumar, J. Larson, D. Lykov, P. Minssen, Y. Sun, Y. Alexeev, J. M. Dreiling, J. P. Gaebler, T. M. Gatterman, J. A. Gerber, K. Gilmore, D. Gresh, N. Hewitt, C. V. Horst, S. Hu, J. Johansen, M. Matheny, T. Mengle, M. Mills, S. A. Moses, B. Neyenhuis, P. Siegfried, R. Yalovetzky, and M. Pistoia, Evidence of scaling advantage for the quantum approximate optimization algorithm on a classically intractable problem, Science Advances **10**, eadm6761 (2024).

[18] R. Orús, A practical introduction to tensor networks: Matrix product states and projected entangled pair states, Annals of Physics **349**, 117 (2014).

[19] P. Silvi, F. Tschirsich, M. Gerster, J. Jünemann, D. Jaschke, M. Rizzi, and S. Montangero, The Tensor Networks Anthology: Simulation techniques for many-body quantum lattice systems, SciPost Phys. Lect. Notes , 8 (2019).

[20] S.-J. Ran, E. Tirrito, C. Peng, X. Chen, L. Tagliacozzo, G. Su, and M. Lewenstein, *Tensor network contractions: methods and applications to quantum many-body systems* (Springer Nature, 2020).

[21] J. I. Cirac, D. Pérez-García, N. Schuch, and F. Verstraete, Matrix product states and projected entangled pair states: Concepts, symmetries, theorems, Rev. Mod. Phys. **93**, 045003 (2021).

[22] M. C. Bañuls, Tensor network algorithms: A route map, Annual Review of Condensed Matter Physics **14**, 173 (2023).

[23] R. Orús, Tensor networks for complex quantum systems, Nature Reviews Physics **1**, 538 (2019).

[24] M. S. Rudolph, J. Miller, D. Motlagh, J. Chen, A. Acharya, and A. Perdomo-Ortiz, Synergistic pretraining of parametrized quantum circuits via tensor networks, Nature Communications **14**, 8367 (2023).

[25] B. A. Martin, T. Ayral, F. Jamet, M. J. Rančić, and P. Simon, Combining Matrix Product States and Noisy Quantum Computers for Quantum Simulation (2024), arXiv:2305.19231 [quant-ph].

[26] Y. Kim, A. Eddins, S. Anand, K. X. Wei, E. van den Berg, S. Rosenblatt, H. Nayfeh, Y. Wu, M. Zaletel, K. Temme, and A. Kandala, Evidence for the utility of quantum computing before fault tolerance, Nature **618**, 500–505 (2023).

[27] J. Tindall, M. Fishman, E. M. Stoudenmire, and D. Sels, Efficient Tensor Network Simulation of IBM's Eagle Kicked Ising Experiment, PRX Quantum **5**, 010308 (2024).

[28] T. Begušić, J. Gray, and G. K.-L. Chan, Fast and converged classical simulations of evidence for the utility of quantum computing before fault tolerance, Science Advances **10**, eadk4321 (2024).

[29] S. Patra, S. S. Jahromi, S. Singh, and R. Orús, Efficient tensor network simulation of IBM's largest quantum processors, Phys. Rev. Res. **6**, 013326 (2024).

[30] H.-J. Liao, K. Wang, Z.-S. Zhou, P. Zhang, and T. Xiang, Simulation of IBM's kicked Ising experiment with Projected Entangled Pair Operator (2023), arXiv:2308.03082 [quant-ph].

[31] A. D. King, J. Raymond, T. Lanting, R. Harris, A. Zucca, F. Altomare, A. J. Berkley, K. Boothby, S. Ejtemaee, C. Enderud, E. Hoskinson, S. Huang, E. Ladizinsky, A. J. R. MacDonald, G. Marsden, R. Molavi, T. Oh, G. Poulin-Lamarre, M. Reis, C. Rich, Y. Sato, N. Tsai, M. Volkmann, J. D. Whittaker, J. Yao, A. W. Sandvik, and M. H. Amin, Quantum critical dynamics in a 5,000-qubit programmable spin glass, Nature **617**, 61–66 (2023).

[32] A. D. King, A. Nocera, M. M. Rams, J. Dziarmaga, R. Wiersema, W. Bernoudy, J. Raymond, N. Kaushal, N. Heinsdorf, R. Harris, K. Boothby, F. Altomare, A. J. Berkley, M. Boschnak, K. Chern, H. Christiani, S. Cibere, J. Connor, M. H. Dehn, R. Deshpande, S. Ejtemaee, P. Farré, K. Hamer, E. Hoskinson, S. Huang, M. W. Johnson, S. Kortas, E. Ladizinsky, T. Lai, T. Lanting, R. Li, A. J. R. MacDonald, G. Marsden, C. C. McGeoch, R. Molavi, R. Neufeld, M. Norouzpour, T. Oh, J. Pasvolsky, P. Poitras, G. Poulin-Lamarre, T. Prescott, M. Reis, C. Rich, M. Samani, B. Sheldan, A. Smirnov, E. Sterpka, B. T. Clavera, N. Tsai, M. Volkmann, A. Whiticar, J. D. Whittaker, W. Wilkinson, J. Yao, T. J. Yi, A. W. Sandvik, G. Alvarez, R. G. Melko, J. Carrasquilla, M. Franz, and M. H. Amin, Computational supremacy in quantum simulation (2024), arXiv:2403.00910 [quant-ph].

[33] Z.-Y. Han, J. Wang, H. Fan, L. Wang, and P. Zhang, Unsupervised Generative Modeling Using Matrix Product States, Phys. Rev. X **8**, 031012 (2018).

[34] J. Lopez-Piqueres, J. Chen, and A. Perdomo-Ortiz, Symmetric tensor networks for generative modeling and constrained combinatorial optimization, Machine Learning: Science and Technology **4**, 035009 (2023).

[35] J. Alcazar, M. Ghazi Vakili, C. B. Kalayci, and A. Perdomo-Ortiz, Enhancing combinatorial optimization with classical and quantum generative models, Nature Communications **15**, 2761 (2024).

[36] S. Mugel, C. Kuchkovsky, E. Sánchez, S. Fernández-Lorenzo, J. Luis-Hita, E. Lizaso, and R. Orús, Dynamic portfolio op-

timization with real datasets using quantum processors and quantum-inspired tensor networks, Phys. Rev. Res. **4**, 013006 (2022).
[37] T. Hao, X. Huang, C. Jia, and C. Peng, A Quantum-Inspired Tensor Network Algorithm for Constrained Combinatorial Optimization Problems, Frontiers in Physics **10**, 10.3389/fphy.2022.906590 (2022).
[38] S. Patra, S. Singh, and R. Orús, Projected Entangled Pair States with flexible geometry (2024), arXiv:2407.21140 [cond-mat.str-el].
[39] E. Pelofske, A. Bärtschi, and S. Eidenbenz, Quantum annealing vs. qaoa: 127 qubit higher-order ising problems on nisq computers, in *High Performance Computing*, edited by A. Bhatele, J. Hammond, M. Baboulin, and C. Kruse (Springer Nature Switzerland, Cham, 2023) pp. 240–258.
[40] E. Pelofske, A. Bärtschi, and S. Eidenbenz, Short-depth QAOA circuits and quantum annealing on higher-order ising models, npj Quantum Information **10**, 1–19 (2024).
[41] N. Sachdeva, G. S. Hartnett, S. Maity, S. Marsh, Y. Wang, A. Winick, R. Dougherty, D. Canuto, Y. Q. Chong, M. Hush, P. S. Mundada, C. D. B. Bentley, M. J. Biercuk, and Y. Baum, Quantum optimization using a 127-qubit gate-model IBM quantum computer can outperform quantum annealers for non-trivial binary optimization problems (2024), arXiv:2406.01743 [quant-ph].
[42] M. Demirplak and S. A. Rice, Adiabatic Population Transfer with Control Fields, The Journal of Physical Chemistry A **107**, 9937 (2003).
[43] M. V. Berry, Transitionless quantum driving, Journal of Physics A: Mathematical and Theoretical **42**, 365303 (2009).
[44] X. Chen, A. Ruschhaupt, S. Schmidt, A. del Campo, D. Guéry-Odelin, and J. G. Muga, Fast Optimal Frictionless Atom Cooling in Harmonic Traps: Shortcut to Adiabaticity, Phys. Rev. Lett. **104**, 063002 (2010).
[45] A. del Campo, Shortcuts to adiabaticity by counterdiabatic driving, Phys. Rev. Lett. **111**, 100502 (2013).
[46] P. Chandarana, N. N. Hegade, K. Paul, F. Albarrán-Arriagada, E. Solano, A. del Campo, and X. Chen, Digitized-counterdiabatic quantum approximate optimization algorithm, Phys. Rev. Res. **4**, 013141 (2022).
[47] N. N. Hegade, X. Chen, and E. Solano, Digitized counter-diabatic quantum optimization, Phys. Rev. Res. **4**, L042030 (2022).
[48] A. G. Cadavid, A. Dalal, A. Simen, E. Solano, and N. N. Hegade, Bias-field digitized counterdiabatic quantum optimization (2024), arXiv:2405.13898 [quant-ph].
[49] IBM Quantum, (2024), https://quantum.ibm.com/.
[50] D-Wave Systems, (2024), https://www.dwavesys.com/.
[51] U. Schollwöck, The density-matrix renormalization group in the age of matrix product states, Annals of Physics **326**, 96 (2011).
[52] R. Battiti, Maximum satisfiability problem, in *Encyclopedia of Optimization*, edited by C. A. Floudas and P. M. Pardalos (Springer US, Boston, MA, 2009) pp. 2035–2041.
[53] N. N. Hegade, K. Paul, F. Albarrán-Arriagada, X. Chen, and E. Solano, Digitized adiabatic quantum factorization, Phys. Rev. A **104**, L050403 (2021).
[54] A. Robert, P. K. Barkoutsos, S. Woerner, and I. Tavernelli, Resource-efficient quantum algorithm for protein folding, npj Quantum Information **7**, 1–5 (2021).
[55] P. Chandarana, N. N. Hegade, I. Montalban, E. Solano, and X. Chen, Digitized Counterdiabatic Quantum Algorithm for Protein Folding, Phys. Rev. Appl. **20**, 014024 (2023).
[56] A. Crisanti and H. J. Sommers, The spherical p-spin interaction spin glass model: the statics, Zeitschrift für Physik B Condensed Matter **87**, 341–354 (1992).
[57] M. Kolodrubetz, D. Sels, P. Mehta, and A. Polkovnikov, Geometry and non-adiabatic response in quantum and classical systems, Physics Reports **697**, 1 (2017).
[58] D. Sels and A. Polkovnikov, Minimizing irreversible losses in quantum systems by local counterdiabatic driving, Proceedings of the National Academy of Sciences **114**, E3909 (2017).
[59] P. W. Claeys, M. Pandey, D. Sels, and A. Polkovnikov, Floquet-Engineering Counterdiabatic Protocols in Quantum Many-Body Systems, Phys. Rev. Lett. **123**, 090602 (2019).
[60] T. Hatomura and K. Takahashi, Controlling and exploring quantum systems by algebraic expression of adiabatic gauge potential, Phys. Rev. A **103**, 012220 (2021).
[61] K. Takahashi and A. del Campo, Shortcuts to Adiabaticity in Krylov Space, Phys. Rev. X **14**, 011032 (2024).
[62] S. V. Romero, X. Chen, G. Platero, and Y. Ban, Optimizing edge-state transfer in a Su-Schrieffer-Heeger chain via hybrid analog-digital strategies, Phys. Rev. Appl. **21**, 034033 (2024).
[63] A. Dalal, I. Montalban, N. N. Hegade, A. G. Cadavid, E. Solano, A. Awasthi, D. Vodola, C. Jones, H. Weiss, and G. Füchsel, Digitized Counterdiabatic Quantum Algorithms for Logistics Scheduling (2024), arXiv:2405.15707 [quant-ph].
[64] L. Hormozi, E. W. Brown, G. Carleo, and M. Troyer, Nonstoquastic hamiltonians and quantum annealing of an ising spin glass, Physical review B **95**, 184416 (2017).
[65] N. N. Hegade, K. Paul, Y. Ding, M. Sanz, F. Albarrán-Arriagada, E. Solano, and X. Chen, Shortcuts to Adiabaticity in Digitized Adiabatic Quantum Computing, Phys. Rev. Appl. **15**, 024038 (2021).
[66] M. Suzuki, Fractal decomposition of exponential operators with applications to many-body theories and Monte Carlo simulations, Physics Letters A **146**, 319 (1990).
[67] P. V. Sriluckshmy, V. Pina-Canelles, M. Ponce, M. G. Algaba, F. Šimkovic IV, and M. Leib, Optimal, hardware native decomposition of parameterized multi-qubit Pauli gates, Quantum Science and Technology **8**, 045029 (2023).
[68] M. G. Algaba, P. V. Sriluckshmy, M. Leib, and F. Šimkovic IV, Low-depth simulations of fermionic systems on square-grid quantum hardware, Quantum **8**, 1327 (2024).
[69] T. Graß, Quantum Annealing with Longitudinal Bias Fields, Phys. Rev. Lett. **123**, 120501 (2019).
[70] T. Grass, Quantum Annealing Sampling with a Bias Field, Phys. Rev. Appl. **18**, 044036 (2022).
[71] D. J. Egger, J. Mareček, and S. Woerner, Warm-starting quantum optimization, Quantum **5**, 479 (2021).
[72] F. Truger, J. Barzen, M. Bechtold, M. Beisel, F. Leymann, A. Mandl, and V. Yussupov, Warm-Starting and Quantum Computing: A Systematic Mapping Study, ACM Comput. Surv. **56**, 10.1145/3652510 (2024).
[73] P. K. Barkoutsos, G. Nannicini, A. Robert, I. Tavernelli, and S. Woerner, Improving Variational Quantum Optimization using CVaR, Quantum **4**, 256 (2020).
[74] M. Fishman, S. R. White, and E. M. Stoudenmire, The ITensor Software Library for Tensor Network Calculations, SciPost Phys. Codebases , 4 (2022).
[75] R. Impagliazzo and R. Paturi, On the Complexity of k-SAT, J. Comput. Syst. Sci. **62**, 367–375 (2001).
[76] H. Philathong, V. Akshay, K. Samburskaya, and J. Biamonte, Computational phase transitions: benchmarking Ising machines and quantum optimisers, Journal of Physics: Complexity **2**, 011002 (2021).
[77] B. Zhang, A. Sone, and Q. Zhuang, Quantum computational phase transition in combinatorial problems, npj Quantum Infor-

mation **8**, 87 (2022).
[78] H. Philathong, V. Akshay, I. Zacharov, and J. Biamonte, Computational phase transition signature in Gibbs sampling, Journal of Physics: Complexity **4**, 045010 (2023).
[79] H. Ishikawa, Transformation of General Binary MRF Minimization to the First-Order Case, IEEE Transactions on Pattern Analysis and Machine Intelligence **33**, 1234 (2011).
[80] M. Anthony, E. Boros, Y. Crama, and A. Gruber, Quadratic reformulations of nonlinear binary optimization problems, Mathematical Programming **162**, 115–144 (2017).
[81] N. Dattani, Quadratization in discrete optimization and quantum mechanics (2019), arXiv:1901.04405 [quant-ph].
[82] Gurobi Optimization, LLC, Gurobi Optimizer Reference Manual (2024).
[83] I. I. Cplex, V12.10.0: User's Manual for CPLEX, International Business Machines Corporation **46**, 157 (2009).
[84] J. Eisert, M. Cramer, and M. B. Plenio, Colloquium: Area laws for the entanglement entropy, Rev. Mod. Phys. **82**, 277 (2010).
[85] J. Rodríguez-Laguna, Quantum wavefunction annealing of spin glasses on ladders, Journal of Statistical Mechanics: Theory and Experiment **2007**, P05008 (2007).
[86] J. Rodríguez-Laguna, Density matrix renormalization on random graphs and the quantum spin-glass transition, Journal of Physics A: Mathematical and Theoretical **40**, 12043 (2007).